

Image Simulation for 3-FOV Daytime Star Sensor based on Ray Tracing

Feng Wu*, Xifang Zhu, Ruxi Xiang, Xiaoyan Jiang, Qingquan Xu, Gong Chen, Tao Wu

School of Electrical & Photoelectronic Engineering, Changzhou Institute of Technology,
Changzhou 213032, China (dermindee@gmail.com)

Abstract

Daytime star sensor provides accurate navigation information to air vehicles flying near the ground all day long. To filter out the strong background radiation in the atmospheric environment, the daytime star sensor has been designed with multiple infrared star cameras. The new design, known as the star sensor with multiple fields of view (FOV), represents the future directions for modern star sensors. The development of the daytime star sensor requires a huge number of star maps, which can be efficiently produced by computer-aided image simulation. In light of the above, this paper proposes an image simulation method for the 3-FOV star sensor, and analyses its structure and working principle. Then, the author designed a simulation framework consisting of an observed star catalogue, an observed start calculation module, a ray tracing module, and an image output module. Specifically, the observed star catalogue was created after studying and processing the Two Micron All-Sky Survey (2MASS) star catalogue. Moreover, the entry of rays into the optical system, composed of spherical or aspherical optical surfaces, in the 3-FOV daytime star sensor was explained in details, the pixel energy on the image plane was calculated to generate the simulated star maps, and the simulation experiments were carried out to verify the feasibility of the proposed image simulation method.

Key words

Daytime star sensor, Star catalogue, Ray tracing, Observed stars, Image simulation, Aspherical surface.

1. Introduction

Star sensors provide accurate attitude information to air vehicles by capturing observed stars

and processing star maps. Most of the existing star sensors work in the visible bands outside the earth. Under the protection of baffles, they are seldom affected by strong stray light. The attitude calculation is smoothed by the high signal-to-noise ratio of the star maps. The daytime star sensor has been designed to provide air vehicles flying 24/7 near the ground with accurate navigation information. To filter out the strong background radiation in the atmospheric environment, the daytime star sensor often works in the infrared bands with a structure called the multiple fields of view (FOV). Whereas the traditional star sensor contains only one star camera, the multi-FOV daytime star sensor has several identical star cameras, representing the future directions for modern star sensors. With the replacement of the large FOV with several small FOVs, the multi-FOV daytime star sensor outperforms the traditional star sensor in sensing accuracy, layout flexibility, and resistance to background radiation. Typical applications of the new star sensor include the double-FOV star sensor for ship attitude measurement adopted by maritime satellite measuring and control department of China [1], and the three-FOV star sensor in Daystar (Microcosm Inc.) and Hydra (Sodern).

Similar to that of traditional star sensor, the development of the daytime star sensor requires a huge number of star maps to check the feasibility or performance of optical system design [4], star image extraction [5], guide star selection, star identification [6], and attitude estimation [7]. Since it is time-consuming and cost-ineffective to produce the star maps by photo-taking, the computer-aided image simulation has been developed, offering a convenient method for star map generation.

The remainder of this paper is organized as follows. Section 2 introduces the structure of the 3-FOV daytime star sensor, establishes the coordinate systems for the body and sub-systems, and discusses the relationship between the these coordinate systems; Section 3 designs a simulation framework, consisting of an observed star catalogue, an observed start calculation module, a ray tracing module, and an image output module; moreover, the observed star catalogue was created after studying and processing the Two Micron All-Sky Survey (2MASS) star catalogue, the entry of rays into the optical system, composed of spherical or aspherical optical surfaces, in the 3-FOV daytime star sensor was explained in details, and the ray tracing formulas were derived; Section 4 carries out the simulation experiments; Section 5 wraps up this research with some meaningful conclusions.

2. Structure of the 3-FOV Daytime Star Sensor

The 3-FOV daytime star sensor contains three identical star cameras sharing a common processing unit. Each of the star cameras captures the observed stars in its FOV via its optical system, maps them onto the image plane, and thus produces the star maps. After receiving the star

maps from the three star cameras, the processing unit combines them to identify stars and measure attitude.

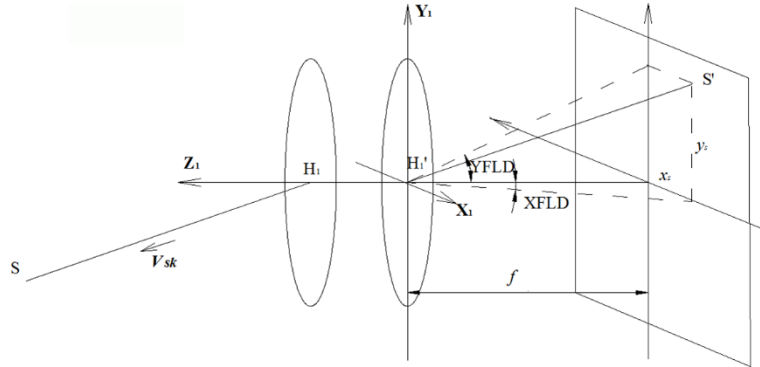


Fig.1. Sub-system Coordinate Systems

The first step of the study on the 3-FOV daytime star sensor is to set up the coordinate systems for the body and the three sub-systems. The sub-systems correspond to the three star cameras. In this research, the body coordinate system is denoted as $O_b-X_bY_bZ_b$ and the three sub-system coordinate systems are denoted as $O_k-X_kY_kZ_k$, where k is 1, 2 or 3 depending on the specific star camera. The sub-system coordinate systems $O_k-X_kY_kZ_k$ were established in reference to the previous studies [8] because each star camera works exactly the same with a traditional single-FOV star sensor. The system $O_1-X_1Y_1Z_1$ is illustrated in Figure 1, where H_1 and H_1' are the principal points in the object space and the image space, respectively, and f is the focal length of the camera. The origin O_1 is located at H_1' ; the axis O_1Z_1 coincides with the optical axis and points to the sky; the axes O_1X_1 and O_1Y_1 are parallel to the row and column of the image plane, respectively.

Assuming that an observed star S is mapped as S' by the k -th star camera, and that the coordinate of S' is $(x_s, y_s, -f)$ in the sub-system $O_k-X_kY_kZ_k$, then the direction cosine of the vector H_kS is:

$$\vec{V}_{sk} = \begin{bmatrix} V_{sk1} \\ V_{sk2} \\ V_{sk3} \end{bmatrix} = \frac{-1}{\sqrt{x_s^2 + y_s^2 + f^2}} \begin{bmatrix} x_s \\ y_s \\ -f \end{bmatrix} \quad (1)$$

The field angles $XFLD$ along O_kX_k and $YFLD$ along O_kY_k are:

$$XFLD = -\text{tg}^{-1}\left(\frac{V_{sk1}}{V_{sk3}}\right), YFLD = -\text{tg}^{-1}\left(\frac{V_{sk2}}{V_{sk3}}\right) \quad (2)$$

In view of the symmetrical arrangement of the three star cameras, $O_b-X_bY_bZ_b$ in Figure 2 was taken as the body coordinate system with the intersection of axes Z_1 , Z_2 and Z_3 as the origin O_b . Let φ denote the equal angles between axis Z_b and axes Z_1 , Z_2 and Z_3 , and τ denote the angle between planes $X_1O_1Z_1$ and $X_bO_bZ_b$. The projections of axes Z_1 , Z_2 or Z_3 in the plane $X_bO_bY_b$ are separated by 120° . As shown in Figure 2, φ determines the relative location among the three optical systems.

If axis O_bZ_b points to (α_c, δ_c) in the inertial coordinate system $O_i-X_iY_iZ_i$, then $O_i-X_iY_iZ_i$ must coincide with the body coordinate system $O_b-X_bY_bZ_b$ after rotating three times in sequence. First, $O_i-X_iY_iZ_i$ rotates by α_c around axis O_iZ_i from $+O_iX_i$ to $+O_iY_i$, resulting in the coordinate system $O_i-X'Y'Z'$; then, $O_i-X'Y'Z'$ rotates by $90^\circ-\delta_c$ around axis O_iY' from $+O_iZ'$ to $+O_iX'$, turning into the coordinate system $O_i-X''Y''Z''$; Finally, $O_i-X''Y''Z''$ rotates by θ around axis O_iZ'' and ends up as the body coordinate system $O_b-X_bY_bZ_b$. The angle θ depends on the direction of axis O_bX_b or axis O_bY_b . Similarly, the body coordinate system $O_b-X_bY_bZ_b$ can coincide with sub-system coordinate systems $O_k-X_kY_kZ_k$ after rotating twice in sequence. First, $O_b-X_bY_bZ_b$ rotates by $\tau+(k-1)*120^\circ$ around axis O_bZ_b from $+O_bX_b$ to $+O_bY_b$, forming $O_b-X_k'Y_k'Z_k'$; then, the new coordinate system rotates by φ around axis O_bZ_b from $+O_bX_b$ to $+O_bY_b$, creating a coordinate system which coincides with the sub-system coordinate system $O_k-X_kY_kZ_k$.

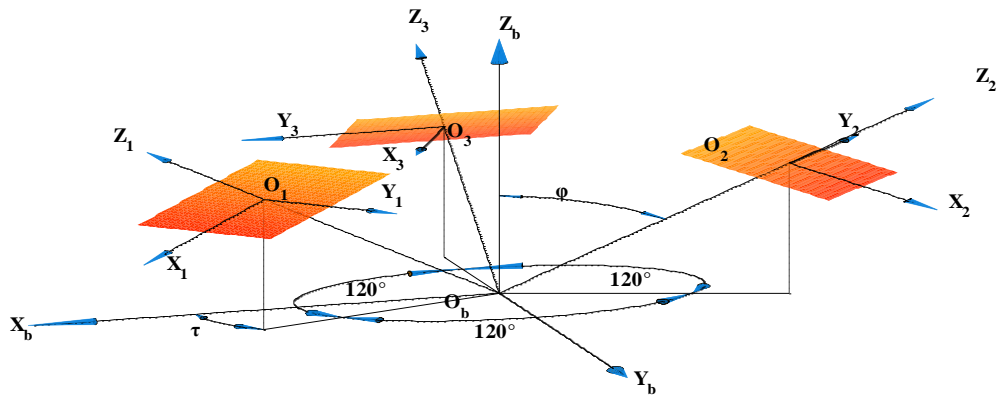


Fig.2. Relationships between the Coordinate Systems

If the coordinate of the star S in the inertial coordinate system $O_i-X_iY_iZ_i$ is (α, δ) , the direction cosine of the star in each sub-system coordinate system can be derived based on the relationships of the coordinate systems $O_i-X_iY_iZ_i$, $O_b-X_bY_bZ_b$, and $O_k-X_kY_kZ_k$:

$$\begin{aligned}
\begin{bmatrix} V_{sk1} \\ V_{sk2} \\ V_{sk3} \end{bmatrix} &= \begin{bmatrix} \cos \varphi & 0 & -\sin \varphi \\ 0 & 1 & 0 \\ \sin \varphi & 0 & \cos \varphi \end{bmatrix} \begin{bmatrix} \cos[(k-1)*120^\circ + \tau] & \sin[(k-1)*120^\circ + \tau] & 0 \\ -\sin[(k-1)*120^\circ + \tau] & \cos[(k-1)*120^\circ + \tau] & 0 \\ 0 & 0 & 1 \end{bmatrix} \times \\
&\begin{bmatrix} \cos \theta & \sin \theta & 0 \\ -\sin \theta & \cos \theta & 0 \\ 0 & 0 & 1 \end{bmatrix} \begin{bmatrix} \cos(90 - \delta_c) & 0 & -\sin(90 - \delta_c) \\ 0 & 1 & 0 \\ \sin(90 - \delta_c) & 0 & \cos(90 - \delta_c) \end{bmatrix} \begin{bmatrix} \cos \alpha_c & \sin \alpha_c & 0 \\ -\sin \alpha_c & \cos \alpha_c & 0 \\ 0 & 0 & 1 \end{bmatrix} \begin{bmatrix} \cos \alpha \cos \delta \\ \sin \alpha \cos \delta \\ \sin \delta \end{bmatrix}
\end{aligned}
\tag{3}$$

If the direction cosine of a vector in $O_k\text{-}X_kY_kZ_k$ is $\{V_{k1}, V_{k2}, V_{k3}\}$, it can be expressed as below in the inertial coordinate:

$$\begin{aligned}
\begin{bmatrix} V_1 \\ V_2 \\ V_3 \end{bmatrix} &= \begin{bmatrix} \cos \alpha_c & -\sin \alpha_c & 0 \\ \sin \alpha_c & \cos \alpha_c & 0 \\ 0 & 0 & 1 \end{bmatrix} \begin{bmatrix} \cos(90^\circ - \delta_c) & 0 & \sin(90^\circ - \delta_c) \\ 0 & 1 & 0 \\ -\sin(90^\circ - \delta_c) & 0 & \cos(90^\circ - \delta_c) \end{bmatrix} \begin{bmatrix} \cos \theta & -\sin \theta & 0 \\ \sin \theta & \cos \theta & 0 \\ 0 & 0 & 1 \end{bmatrix} \times \\
&\begin{bmatrix} \cos[(k-1)*120^\circ + \tau] & -\sin[(k-1)*120^\circ + \tau] & 0 \\ \sin[(k-1)*120^\circ + \tau] & \cos[(k-1)*120^\circ + \tau] & 0 \\ 0 & 0 & 1 \end{bmatrix} \begin{bmatrix} \cos \varphi & 0 & \sin \varphi \\ 0 & 1 & 0 \\ -\sin \varphi & 0 & \cos \varphi \end{bmatrix} \begin{bmatrix} V_{k1} \\ V_{k2} \\ V_{k3} \end{bmatrix}
\end{aligned}
\tag{4}$$

3. Image Simulation by Ray Tracing

The image simulation of the 3-FOV daytime star sensor was implemented in the imaging steps of a real system. When a star appears in the FOV of a star camera, it is captured and mapped onto the image plane. Then, the simulated star maps can be obtained by ray tracing. Therefore, the author proposed a simulation framework consisting of an observed star catalogue, an observed start calculation module, a ray tracing module, and an image output module. As its name suggests, the observed star catalogue stores the observed stars filtered by the sensitivity of star cameras. The observed star calculation module searches for the stars observed by each star camera. The ray tracing module works in the principles of geometric optics. With the framework, the simulated star maps can be produced by calculating the locations and intensities of the star images.

3.1 Observed Star Catalogue

A star sensor in orbit only captures the stars whose brightness falls in its sensitivity range. The magnitude of the faintest star observed by the star sensor is defined as the limiting magnitude. Prior to simulation, it is necessary to put all observed stars into a catalogue. In this research, the data on stars are extracted from Two Micron All-Sky Survey (2MASS) star catalogue [9]. The 2MASS catalogue contains nearly uniformly distributed stars for the epoch 2000 reference frame in three

near-infrared wavebands, including variable stars, single star, double stars, and multiple stars. For simplicity, only J band is considered in this research. Let us denote the magnitude of single stars, the smallest magnitude of variable stars, the effective magnitude of double stars and multiple stars as M_s , M_v and M_d , respectively. The stars whose M_s , M_v or M_d are no greater than the limiting magnitude were added to the observed star catalogue, together with their star numbers, magnitudes, right ascensions and declinations.

3.2 Observed Star Calculation Module

To prepare for image simulation, the stars captured in the three FOVs were selected. As mentioned in the preceding section, φ and τ determines the layout of the 3-FOV daytime star, and the direction (α_c, δ_c) of axis Z_b in the inertial coordinate system. If these parameters are known, the observed stars can be identified as follows.

First, let us determine the direction of optical axis of each star camera in the inertial coordinate system. If we denote the direction cosine vector of axis Z_k as $\{V_{k1}, V_{k2}, V_{k3}\} = \{0 \ 0 \ 1\}$ in the sub-system coordinate system $O_k-X_kY_kZ_k$, then the vector becomes $\{V_1, V_2, V_3\}$ in the inertial coordinate system according to Equation (4), and the axis Z_k points to $(\alpha_{zk}, \delta_{zk})$ in Equation (5):

$$\delta_{zk} = \sin^{-1}(V_3), \quad \alpha_{zk} = \begin{cases} \sin^{-1}(V_2 / \cos(\delta_{zk})) & \text{if } V_1 > 0, V_2 > 0 \\ \cos^{-1}(V_1 / \cos(\delta_{zk})) & \text{if } V_1 < 0, V_2 > 0 \\ 360^\circ + \sin^{-1}(V_2 / \cos(\delta_{zk})) & \text{if } V_1 > 0, V_2 < 0 \\ 180^\circ + \text{tg}^{-1}(V_2 / V_1) & \text{if } V_1 < 0, V_2 < 0 \end{cases} \quad (5)$$

If w_m is the FOV corresponding to the diagonal line of the optical system image plane, the stars satisfying Equation (6) should be the candidate stars.

$$|\delta - \delta_{zk}| \leq w_m \quad (6)$$

where α and δ are the right ascension and declination of the star in the inertial coordinate system, respectively.

Similarly, the direction cosine vectors of the candidate stars in the sub-system coordinate systems $O_k-X_kY_kZ_k$ are calculated according to Equation (3), and their field angles $XFLD$ and $YFLD$ are obtained according to Equation (2).

Whereas the stars observed in the FOV of the k -th camera should satisfy Equation (7), the observed stars appearing in FOV can be determined by filtering the candidate stars by Equation (7).

$$|XFLD| \leq \frac{W_A}{2}, |YFLD| \leq \frac{W_B}{2} \quad (7)$$

3.3 Ray Tracing Module

Ray tracing is the basic method to calculate the aberrations of the optical systems according to the principles of geometric optics. Before arriving at the image plane, the rays emitted from the object were reflected/refracted by one surface after another. The intersections of these rays on the image plane form the image. The rays, each of which carries some energy, ought to be distributed uniformly on the entrance pupil. Hence, the entrance pupil of the k -th star camera was meshed into square grids, and those passing through all grid points were selected from the rays emitted from the observed stars.

Considering the star magnitude and spectrum responses of the sensor, two weights, denoted as W_m and W_w , were introduced to measure the brightness of stars and the spectrum responses of the sensor. Suppose the total number of rays emitted from an observed star is n_{ray} , then the original energy of each ray is $W_m W_w / n_{ray}$.

In this research, only the most common optical system of star sensors is taken into account: the axisymmetric optical system containing spherical or aspherical optical surfaces. A coordinate system was established for each surface. As for the j -th surface, the coordinate system is $\sigma_j - \xi_j \zeta_j \eta_j$. The origin σ_j is located at the vertex, and the axis $\sigma_j \eta_j$ is the symmetric axis coincident to the optical axis. Therefore, the j -th surface can be expressed as:

$$\eta_j = f_j(\xi_j, \zeta_j) = \frac{r_j^2}{R_j + \sqrt{R_j^2 - (1 + K_j)r_j^2}} + \sum_{t=1}^{N_j} A_{j,t} r_j^t \quad (8)$$

where R_j is the curvature radius at the vertex; K_j is the conic constant; $A_{j,t}$ is the aspherical coefficient; $r_j = \sqrt{(\xi_j^2 + \zeta_j^2)}$. The surface is spherical when both K_j and $A_{j,t}$ are zero.

If we denote the distance between the j -th surface and the $(j+1)$ -th surface as d_j , and the refraction indexes of the media before and after the surface as n_j and n_{j+1} , respectively, then the ray tracing procedures can be described as follows.

(1) Let us describe the direction of a ray emitted from an observed star by XFLD and YFLD. Then, its cosine vector $\{l_1, m_1, p_1\}$ can be written as

$$\begin{aligned}
l_1 &= \frac{tg(XFLD)}{\sqrt{tg^2(XFLD) + tg^2(YFLD) + 1}} \\
m_1 &= \frac{tg(YFLD)}{\sqrt{tg^2(XFLD) + tg^2(YFLD) + 1}} \\
p_1 &= \frac{1}{\sqrt{tg^2(XFLD) + tg^2(YFLD) + 1}}
\end{aligned} \tag{9}$$

Suppose the coordinate of the incidence point of the ray on the entrance pupil is $(\xi_0^p, \zeta_0^p, \eta_0^p)$, and the axial distance from the entrance pupil to the 1st optical surface is d_p . Then, the ray will arrive at the point (ξ_1, ζ_1, η_1) on the first optical surface. The point must satisfy the following equation.

$$\frac{\xi_1 - \xi_0^p}{l_1} = \frac{\zeta_1 - \zeta_0^p}{m_1} = \frac{\eta_1 - \eta_0^p}{p_1} \tag{10}$$

The (ξ_1, ζ_1, η_1) can be determined by combining Equations (8)~(10).

(2) Let us calculate the cosine vector $\{l_{j+1}, m_{j+1}, p_{j+1}\}$ of the ray leaving from the j -th surface. Whereas its incidence point on this surface is (ξ_j, ζ_j, η_j) , the normal direction $\{u_j, v_j, w_j\}$ should satisfy the equations below:

$$u_j = \frac{\xi_j}{\sqrt{\xi_j^2 + \zeta_j^2}} \frac{\frac{d\eta_j}{dr_j}}{\sqrt{1 + (\frac{d\eta_j}{dr_j})^2}}, v_j = \frac{\zeta_j}{\sqrt{\xi_j^2 + \zeta_j^2}} \frac{\frac{d\eta_j}{dr_j}}{\sqrt{1 + (\frac{d\eta_j}{dr_j})^2}}, w_j = \frac{-1}{\sqrt{1 + (\frac{d\eta_j}{dr_j})^2}} \tag{11}$$

and

$$\begin{aligned}
l_{j+1} &= \frac{n_j}{n_{j+1}} l_j + u_j \left[\frac{n_j}{n_{j+1}} \cos \mu - \sqrt{1 - \sin^2 \mu \left(\frac{n_j}{n_{j+1}} \right)^2} \right] \\
m_{j+1} &= \frac{n_j}{n_{j+1}} m_j + v_j \left[\frac{n_j}{n_{j+1}} \cos \mu - \sqrt{1 - \sin^2 \mu \left(\frac{n_j}{n_{j+1}} \right)^2} \right] \\
p_{j+1} &= \frac{n_j}{n_{j+1}} p_j + w_j \left[\frac{n_j}{n_{j+1}} \cos \mu - \sqrt{1 - \sin^2 \mu \left(\frac{n_j}{n_{j+1}} \right)^2} \right]
\end{aligned} \tag{12}$$

where $\mu = \cos^{-1}(|l_j u_j + m_j v_j + p_j w_j|)$ is the angle between the normal ray and the incident ray.

(3) If the current j -th surface is the second last surface, let us calculate the incident point $(\xi_{j+1}, \zeta_{j+1}, \eta_{j+1})$ of the ray on the $(j+1)$ -th surface. If j increases by 1, implement Step (2) again; otherwise, return to Step (4). The detailed procedures are as follows.

Suppose the initial coordinate is $(\xi_{j+1,0}, \zeta_{j+1,0}, \eta_{j+1,0})$, and

$$\xi_{j+1,0} = \xi_j, \zeta_{j+1,0} = \zeta_j \text{ and } \eta_{j+1,0} = \eta_j - d_j \quad (13)$$

Let us calculate a new coordinate by invoking Equation (14) repeatedly until the difference between $\eta_{j+1,t+1}$ and $\eta_{j+1,t}$ is so small as to approximate 10^{-6} mm.

$$\begin{aligned} \xi_{j+1,t+1} &= \xi_{j+1,t} + l_{j+1} \frac{f_{j+1}(\xi_{j+1,t}, \zeta_{j+1,t}) - \eta_{j+1,t}}{p_{j+1}} \\ \zeta_{j+1,t+1} &= \zeta_{j+1,t} + m_{j+1} \frac{f_{j+1}(\xi_{j+1,t}, \zeta_{j+1,t}) - \eta_{j+1,t}}{p_{j+1}} \\ \eta_{j+1,t+1} &= f_{j+1}(\xi_{j+1,t}, \zeta_{j+1,t}) \end{aligned} \quad (14)$$

where t is a counter that increases by 1 gradually. Thus, we obtain the incident point location $(\xi_{j+1}, \zeta_{j+1}, \eta_{j+1})$ on the $(j+1)$ -th surface.

(4) Let us calculate the position $(\xi_{image}, \zeta_{image}, \eta_{image})$ of the ray hitting the image plane. The emergent position of the ray from the last surface is $(\xi_{mx}, \zeta_{mx}, \eta_{mx})$, and its direction cosine vector is (l_{mx}, m_{mx}, p_{mx}) . Moreover, the axis distance from this surface to the image plane is d_{mx} . Then, it is possible to derive the following equation.

$$\xi_{image} = \xi_{mx} + l_{mx} \frac{d_{mx} - \eta_{mx}}{p_{mx}}, \zeta_{image} = \zeta_{mx} + m_{mx} \frac{d_{mx} - \eta_{mx}}{p_{mx}}, \eta_{image} = 0 \quad (15)$$

In this way, the image of every observed star within the FOV of the k -th star camera can be achieved by tracing a number of rays with several wavelengths in the spectrum range.

3.4 Image Output Module

The star images on the image plane are received by the CCD or the APS whose surfaces are made up of pixels. All rays hitting the same pixel will be accumulated during the exposure and represented by a grey value after photovoltaic conversion and analogue-digital conversion. Therefore, all ray energies in the same pixel should be added together and digitalized to produce a digital image.

4. Simulation Results and Analysis

Our simulation utilizes the refractive optical system mentioned in [10]. The daytime star sensor is composed of 3 optical systems with the focal length of 100mm, the FOV of 5.74° and F/# of 2. The designed working wavelength falls between 3~5 μm . Each optical system contains four lenses, in which the back surface of the first lens and the front surface of the third lens are aspherical, and the other surfaces are spherical. It is deduced that the optical system has a FOV of $4.06^\circ \times 4.06^\circ$. The image sensor contains $1,024 \times 1,024$ pixels, each of which is $6.9\mu\text{m} \times 6.9\mu\text{m}$ in size. 6,223 stars in the J band, excluding variable and double stars, were extracted from 2MASS with the limiting magnitude of 4Mv.

Tab.1. Orientations of Axis Z_k of the Three Sub-system Coordinate Systems

Axis	$Z_b(^{\circ})$	$Z_1(^{\circ})$	$Z_2(^{\circ})$	$Z_3(^{\circ})$
RA	30	336.51	47.12	80.68
DEC	20	20.17	-27.17	50.47

In the experiment, φ and τ , the determinants of the layout of the 3-FOV daytime star sensor, are set to 50° and 20° , respectively. Figure 3 shows the simulated images when the orientation (α_c , δ_c) of axis Z_b is (30° , 20°) in the inertial coordinate system. Table 1 lists the orientations of axis Z_k of the three sub-system coordinate systems. As shown in Figure 3, the first sub-system captured no star, while the other two sub-systems captured over two stars each. The catalogue ID, magnitude, right ascension and declination of these stars are presented in Table 2. The author calculated the ideal position of the stars according to the imaging theory of ideal optical systems, and obtained their centroid locations by applying the advanced star extraction algorithm. The results show that the biggest error in image simulation is less than $4\mu\text{m}$, no greater than one pixel.

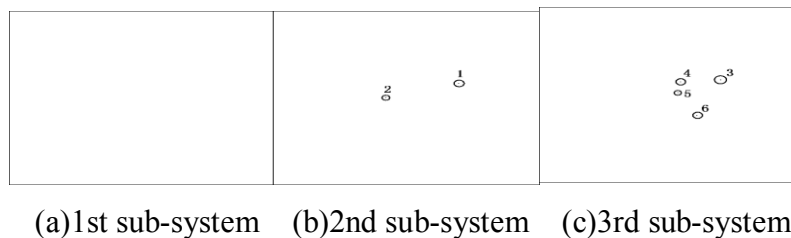


Fig.3. Simulated Star Maps

Tab.2. Positions of the Observed Stars in Sub-system Coordinate Systems and the Inertial Coordinate System

No	ID	Mv	RA (°)	DEC (°)	Ideal position (mm)		Centroid position (mm)		Δ (μm)
					x	y	x	y	
1	1943	2.572	48.02	-28.99	3.1787	1.3724	3.1754	1.3709	3.62
2	2052	3.341	47.16	-26.45	-1.2630	0.0567	-1.2617	0.0566	1.30
3	5407	3.259	81.90	48.71	3.0677	1.4075	3.0645	1.4059	3.58
4	5446	2.665	78.99	49.55	0.5942	1.2172	0.5935	1.2158	1.57
5	5469	3.502	81.77	50.12	0.4350	0.2185	0.4345	0.2182	0.58
6	5477	3.334	80.88	50.22	1.5905	-1.9128	1.5888	-1.9109	2.55

Conclusions

Computer-aided star map simulation brings great convenience to star map generation, and gives birth to the research on daytime star sensors. Based on the structure of the 3-FOV daytime star sensor, the simulated digital images can be obtained when the observed stars are mapped onto the image planes by tracing rays. With a pre-established observed star catalogue, the image of the observed stars can be simulated successfully by tracing rays through optical systems containing spherical and aspherical surfaces based on the principles of geometric optics. The proposed simulation method is proved as a simple and practical way to produce digital star maps.

Acknowledgements

This research is sponsored by National Natural Science Foundation of China (Grant No. 61640420); Cooperative Innovation Fund Project of Jiangsu Province (Grant No. BY2016031-05); Feature Specialty (Electrical Engineering & Automatization) Construction Project of Jiangsu Province, Phase I; Key Specialty (Electrical Engineering) Construction Project of Jiangsu Province; Key Construction Lab of Special Motor Research and Application of Universities and Colleges of Jiangsu Province; Natural Science Found of Universities and Colleges in Jiangsu Province (Grant No. 15KJD510004); Undergraduate Training Programs for Innovation and Entrepreneurship of Jiangsu Province (Grant No. 201711055004Z).

References

1. B. Liu, W.K. Zhu, T.S. Zhang, L. Yang, J.M. Guo, Determination of ship attitude based on dual star sensors, 2014, *Optics & Precision Engineering*, vol. 22, no. 3, pp. 569-575.
2. N. Truesdale, K. Dinkel, Z. Dischner, J. Diller, Daystar: Modeling and testing a daytime star tracker for high altitude balloon observatories, 2013, *Advances in the Astronautical Sciences*, vol. 149, pp. 47-61.

3. L. Blarre, N. Perrimon, S. Airey, New multiple head Star Sensor (HYDRA) description and development status: a highly autonomous, accurate and very robust system to pave the way for gyroless very accurate AOCS systems, 2005, Proc. AIAA Guidance, Navigation, and Control Conference, pp 817–825.
4. X. Zhong, G. Jin, Design and simulation of CMOS star sensor lens with large relative aperture and wide field, 2011, Proc. EMEIT, pp. 3194-3197.
5. X.F. Zhu, F. Wu, Q.Q. Xu, A fast star image extraction algorithm for autonomous star sensors, 2012, Proc. SPIE, 2012, Beijing, China, pp. 8558211-8558219.
6. G.J. Zhang., X. Wei, J. Jiang, Full-sky autonomous star identification based on radial and cyclic features of star pattern, 2008, Image Vision Computer, vol. 26, no. 7, pp. 891-897.
7. J.L. Crassidis, F.L. Markley, C. Yang, Survey of nonlinear attitude estimation methods, 2007, Journal of Guidance Control and Dynamics, vol. 30, no. 1, pp.12-28.
8. F. Wu, W.M. Shen, Design and simulation of a novel APS star tracker, 2008, Proc. SPIE, pp 1S1-1S11.
9. S.G. Kleinmann, M.G. Lysaght, W.L. Pughe, The two micron all sky survey, 1994, Experimental Astronomy, vol. 217, no. 1-2, pp. 11-17.
10. P. Li, X. Wang, W. Jin, Dual-band infrared optical system design and image quality evaluation, 2013, Infrared & Laser Engineering, vol. 42, no. 11, pp. 2882-2888.